www.acsnano.org

# Efficient Emission of Highly Polarized Thermal Radiation from a Suspended Aligned Carbon Nanotube Film

Andrea Zacheo, <sup>¶</sup> Shinichiro Matano, <sup>¶</sup> Yui Shimura, Shengjie Yu, Jacques Doumani, Natsumi Komatsu, Junichiro Kono, and Hideyuki Maki\*



Downloaded via RICE UNIV on August 5, 2024 at 18:41:47 (UTC). See https://pubs.acs.org/sharingguidelines for options on how to legitimately share published articles.

Cite This: ACS Nano 2024, 18, 15769-15778



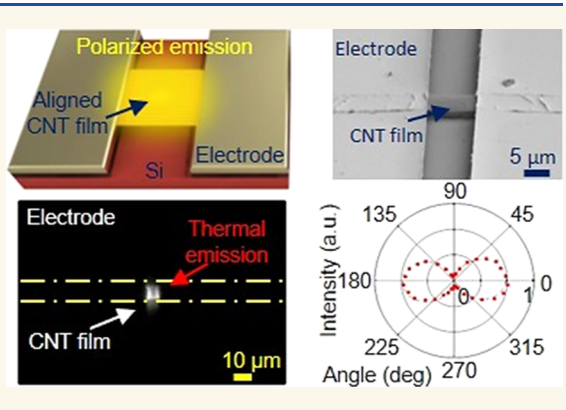
**ACCESS** I

III Metrics & More

Article Recommendations

Supporting Information

ABSTRACT: A polarized light source covering a wide wavelength range is required in applications across diverse fields, including optical communication, photonics, spectroscopy, and imaging. For practical applications, high degrees of polarization and thermal performance are needed to ensure the stability of the radiation intensity and low energy consumption. Here, we achieved efficient emission of highly polarized and broadband thermal radiation from a suspended aligned carbon nanotube film. The anisotropic nature of the film, combined with the suspension, led to a high degree of linear polarization ( $\sim$ 0.9) and great thermal performance. Furthermore, we performed time-resolved measurements of thermal emission from the film, revealing a fast time response of approximately a few microseconds. We also obtained visible light emission from the device and analyzed the film's



mechanical breakdown behavior to improve the emission intensity. Finally, we demonstrated that suspended devices with a constriction geometry can enhance the heating performance. These results show that carbon nanotube film-based devices, as electrically driven thermal emitters of polarized radiation, can play an important role for future development in optoelectronics and spectroscopy.

KEYWORDS: aligned carbon nanotube film, blackbody radiation, light emitter, anisotropy, light polarization, thermal properties

A source of polarized electromagnetic radiation covering a broad spectral range is essential in various fields such as polarimetry, <sup>1</sup> ellipsometry, <sup>2</sup> chiroptical spectroscopy, <sup>3</sup> and magneto-optical sensing. <sup>4,5</sup> Materials' absorption and reflection properties for polarized radiation reflect their anisotropic nature, and optical spectroscopy with polarized radiation can directly reveal materials' anisotropic electronic and vibrational states. Conventionally, linearly polarized narrow-band radiation is obtained from a laser. To obtain polarized broadband radiation, it is required to combine an unpolarized source with an external polarizer, where the entire system becomes bulky. Therefore, the development of a compact source directly generating polarized broadband radiation is desired.

Radiation sources based on nanocarbon materials, such as graphene and carbon nanotubes (CNTs), have emerged as a promising solution for achieving micro/nano-scale emitters of broadband polarized radiation, particularly thermal radiation. Previous research has explored the thermal emission characteristics of CNTs in various configurations, including bundled ropes, 16–18 vertically aligned arrays, 19 and individual wires. Notably, Matano et al. 24,25 have reported polarized

thermal radiation emitted from a film of highly aligned CNTs on a SiO<sub>2</sub>/Si substrate. However, the achieved polarization degree remained unsatisfactory for practical applications, although CNTs have the potential to emit highly polarized radiation. <sup>20–23</sup> In the previous study, the degree of light polarization (DLP), defined as DLP =  $\frac{I_{\parallel} - I_{\perp}}{I_{\parallel} + I_{\perp}}$  (where  $I_{\parallel}$  and  $I_{\perp}$  are the intensities of light polarized in the parallel and perpendicular direction, respectively), was limited to ~0.6, and the thermal performance of the devices was poor due to the presence of the underlying oxide layer.

In this study, we employed highly aligned and suspended CNT films to develop electrically driven emitters capable of

Received: February 21, 2024
Revised: May 6, 2024
Accepted: May 14, 2024
Published: June 3, 2024





producing highly polarized thermal radiation. These films were fabricated using controlled vacuum filtration<sup>26-31</sup> and exhibited anisotropic properties with respect to the CNT alignment direction. <sup>32–37</sup> We observed broadband radiation emitted from the CNT films with wavelengths ranging from the infrared to the visible range. Notably, we achieved an enhanced degree of polarization as high as ~0.9 with the polarization parallel to the CNT alignment direction, independently of the current direction. In addition, film suspension led to a significant improvement in thermal performance because heat dissipation was reduced due to the absence of direct contact with the SiO<sub>2</sub> layer.<sup>38</sup> Furthermore, we evaluated the emission response speed of the devices and found a large anisotropy in the time-resolved thermal response. While obtaining visible light emission, we analyzed the hightemperature behavior and found that a mechanical breakdown of the film improves the light emission intensity. We attribute the breakdown to an evolution of the electric contact resistance at the interface between the CNT film and electrodes during the heating process. We also fabricated suspended devices with constriction and found that the constriction geometry can improve the heating performance.

## **RESULTS AND DISCUSSION**

The anisotropic nature of the CNT films enabled the fabrication and analysis of different configurations of the emitters, as schematically shown in Figure 1a. Specifically, we

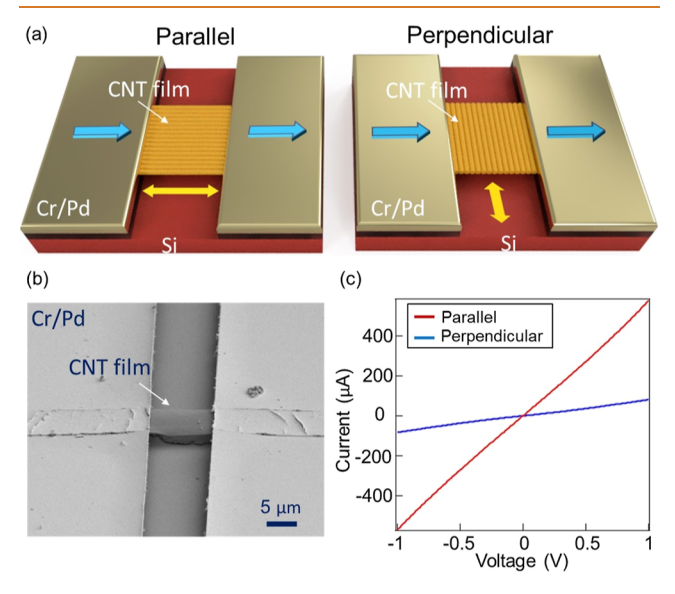


Figure 1. Basic characteristics of a suspended CNT film emitter: (a) schematic diagrams of suspended thermal light emitters in parallel (left) and perpendicular (right) configurations. The yellow arrows show the alignment directions of the CNTs, and the blue solid arrows show the current flow directions. (b) SEM image of suspended CNTs film ( $10 \times 10 \ \mu \text{m}^2$  area) over Si substrate and supported by Cr/Pd electrodes. (c) Current–voltage characteristics of the parallel (red) and perpendicular (blue) devices.

prepared a "parallel" device where the current flow direction coincides with the CNT alignment direction and a "perpendicular" device where the two directions are orthogonal. Each type of device was fabricated using a 100 nm-thick CNT film with an emissive area of  $10 \times 10~\mu\text{m}^2$  suspended over a Si trench with a depth of 1.5  $\mu$ m; see the SEM images in Figure 1b. Additionally, on-substrate (CNT

films lying on a Si/SiO $_2$  1.5  $\mu$ m-thick substrate) devices were fabricated to compare the results with the suspended devices. Strong anisotropy in electrical conductivity was observed in the measured current (I) versus voltage (V) characteristics (see Figure 1c). In the aligned CNT film, the dominant electronic transport mechanism is distinctly different between the parallel and perpendicular directions. At temperatures above 100 K, phonon backscattering is dominant in the parallel transport case, while variable-range hopping is dominant in the perpendicular case. Strong anisotropy has been reported also in thermal conductivity, with an anisotropy ratio between the parallel and perpendicular directions reaching 500.

Figure 2 shows the near-infrared (NIR) emission characteristics under DC voltage of the on-substrate (emission images in Figure 2a,b) and the suspended (emission images in Figure 2e,f) devices for both the "parallel" and "perpendicular" configurations. For the parallel cases, the emission appears broad and uniform along the tube alignment direction due to the larger thermal conductivity, while for the perpendicular cases, the emission is localized at the center of the film, suggesting a larger temperature gradient due to the lower thermal conductivity along the channel direction. Although the suspended perpendicular (Figure 2f) and on-substrate perpendicular (Figure 2b) emission behaviors are similar, suspended parallel emission (Figure 2e) appears slightly different than the on-substrate parallel emission (Figure 2a); it is broader and contains emission spots at the interface with electrodes. This difference is attributed to the distinct heat transport mechanism between the suspended and on-substrate architectures, which clearly affects the light emission shape of the parallel configuration, and is further discussed in the subsequent sections.

To investigate the emission mechanism, we measured the emission spectra of these emitters in the NIR region (Figure 2c,d for the on-substrate device and Figure 2g,h for the suspended device). The spectra of on-substrate devices exhibit an excellent agreement with Planck's law (Figure 2c,d), indicating that the emission originated from thermal radiation. On the other hand, the spectra obtained from the suspended devices show peaks, with an amplitude that increases with increasing emission intensity (Figure 2g,h). The emergence of peaks can be understood by considering an interference phenomenon that occurs from the light emitted from the CNT film and the light reflected back from the Si substrate (Figure 2i), as previously reported in ref 11, 40 for the suspended graphene device. 40 These results suggest that the presence of peaks at specific light-emission wavelengths is significantly influenced by the trench depth from the substrate to the film, indicating that the intensity peaks can be selectively tuned by their trench depths (see Section 2, Supporting Information). We fitted the spectra with the classical Planck's law and a modified law accounting for the effect of the interference for the on-substrate device emission (dashed curves in Figure 2c,d) and suspended device emission, respectively (dashed curves in Figure 2g,h) (see Section 4.3, Supporting Information).

Through curve fitting, we derived the CNT film temperatures during thermal emission. In Figure 3a, we graphically represented the experimentally determined temperatures in relation to the applied electric power. The graph illustrates a linear dependence of the temperature as the input power increases. Comparing parallel and perpendicular devices in both suspended and on-substrate cases, the first immediate

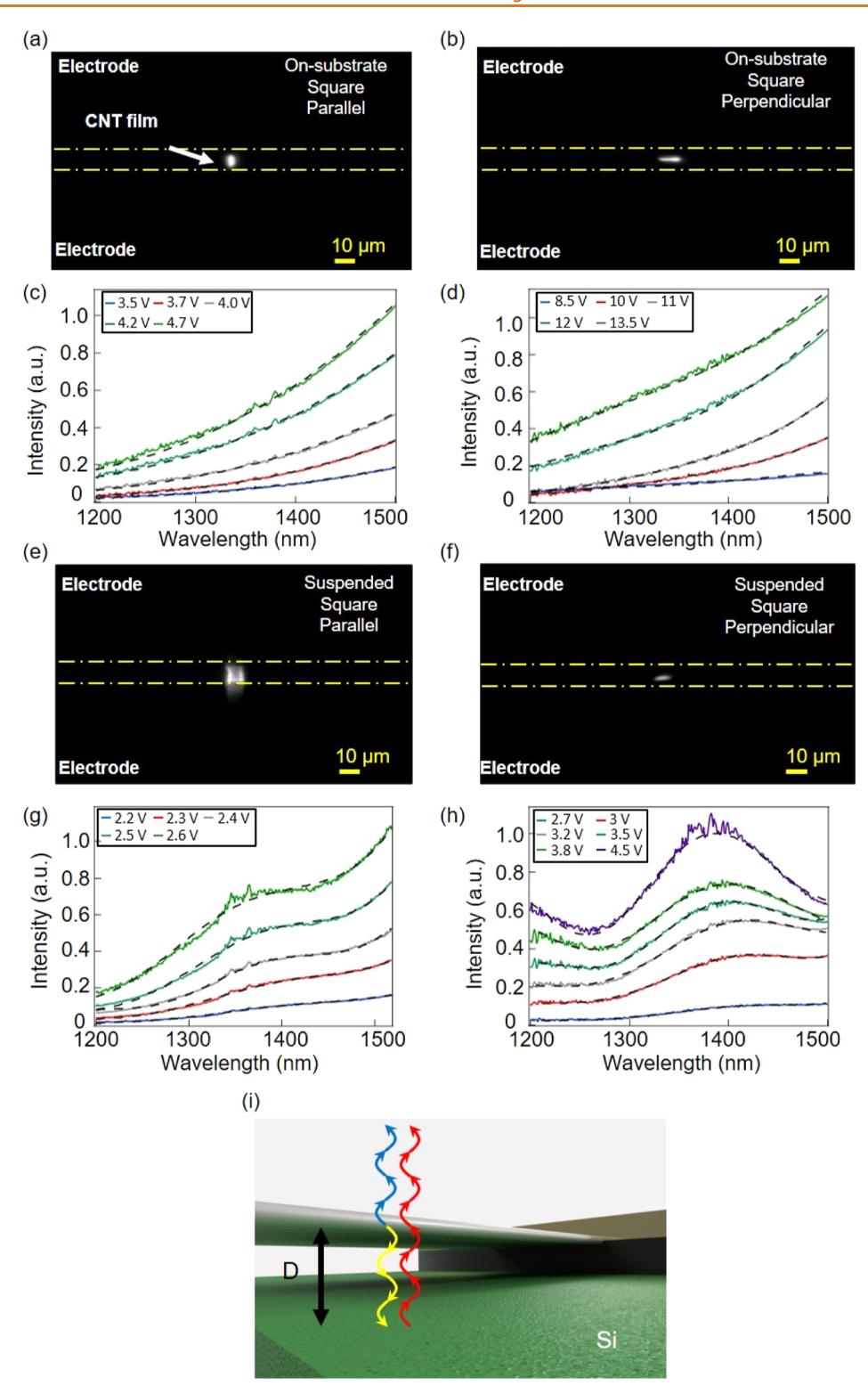


Figure 2. Emission images, spectra, and device temperature of CNTs film thermal light emitters: NIR camera images for (a) parallel and (b) perpendicular on-substrate emitters and (e) parallel and (f) perpendicular suspended emitters. Emission spectra for parallel (c) and perpendicular (d) on-substrate devices, and parallel (g) and perpendicular (h) suspended devices, for various applied voltages. The black dashed curves are fitting curves by Planck's law. The spectra of suspended devices present an oscillatory behavior, with an amplitude that increases with increasing emission intensity, due to the presence of interference phenomenon between the light emitter from the CNTs film and the light reflected from the Si substrate. (i) Schematical representation of the interference effect on the suspended emitters.

result is that the perpendicular devices require less amount of applied power to emit light compared with the parallel devices and this is due to the anisotropic thermal and electrical conductivity of the CNT film (see Section 5 in Supporting

Information). Notably, the suspended devices require lower applied electric power (a few milliWatts) than that in the onsubstrate devices (tens of milliWatts) to obtain the same light emission intensity in parallel and perpendicular devices. This

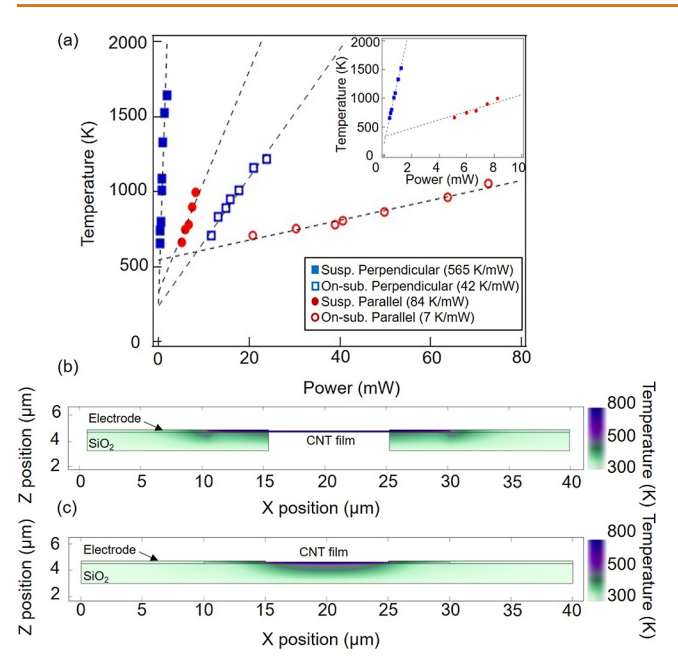


Figure 3. Estimation of the device temperatures and analysis of thermal dynamics: (a) CNT film temperatures as a function of applied power estimated by Planck's law fitting for parallel (red) and perpendicular (blue) on-substrate devices (unfilled markers) and parallel and perpendicular suspended devices (solid markers). The black dashed lines are linear fits that can be used to estimate the thermal performance factor. The suspended structures exhibit larger factors, by 1 order of magnitude overall, than those of the on-substrate structures, in the respective parallel and perpendicular configurations. Finite element method simulation evidences the different dissipation dynamics during the heating of suspended parallel device (b) and on-substrate device (c). The presence of the SiO<sub>2</sub> layer greatly impacts the thermal dynamics of onsubstrate devices and is responsible for an enhanced vertical heat dissipation mechanism. Consequently, this causes on-substrate devices to be less effective at managing heat compared to their suspended counterparts, where heat dissipation primarily occurs through the contact interfaces.

arises from the different heat dissipation mechanisms between the suspended and the on-substrate devices. In the onsubstrate structure, the SiO<sub>2</sub> layer results in enhanced vertical heat dissipation. This makes the on-substrate devices less thermally efficient compared with the suspended ones, where the heat is dissipated only through the contact interfaces. Finite-element simulation results (Figure 3b,c) highlight the different dissipation dynamics during the heating of the two different structures (See Supporting Information for the simulation details). To quantify the improvement achieved by suspension, we determined the values of the thermal performance factor (K·mW<sup>-1</sup>) from the slopes of the line fits to the temperature profiles as the increase in the CNT film temperature per unit applied power. The estimated values are 7 and 42 K·mW<sup>-1</sup> for the parallel and perpendicular on-substrate devices, and 84 and 565 K·mW-1 for the parallel and perpendicular suspended devices. These results indicate that the suspended structure improves the heating performance by 1 order of magnitude compared to the on-substrate configuration in both parallel and perpendicular devices. The heat rate ratios between the suspended and the on-substrate architectures are 12 and 13 for parallel and perpendicular configurations, respectively.

We investigated the polarization of the emitted light in the on-substrate and suspended devices, in both parallel and perpendicular configurations, by utilizing an NIR camera and a polarizer. The primary focus was the detection of the emission intensity of the CNT film. Figure 4a,b shows the angular

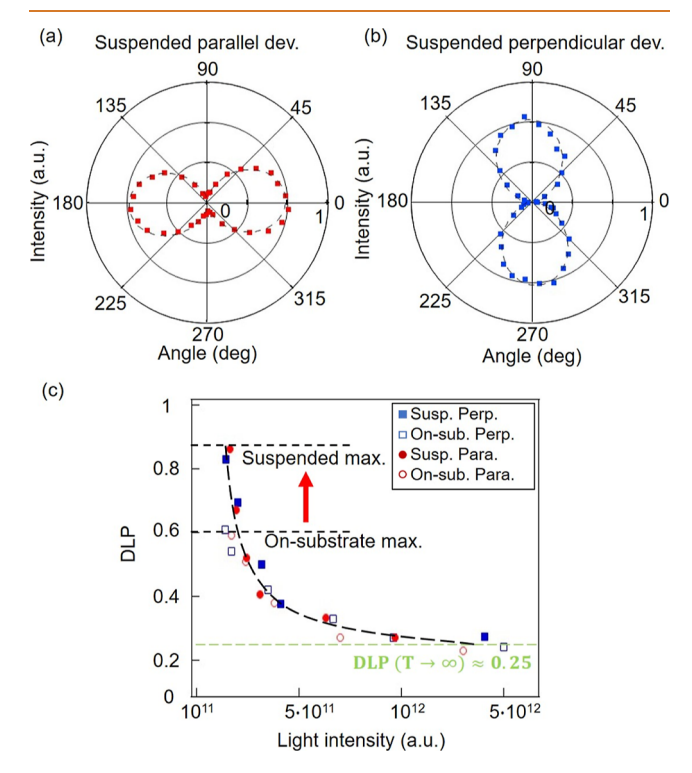


Figure 4. Polarized light emission from suspended CNTs film thermal light emitters: Light polarization dependence of emission intensity from (a) parallel and (b) perpendicular devices. Dotted curves are fits by  $I_{\perp}-(I_{\parallel}+I_{\perp})\cos^2(\vartheta-\varphi)$ . (c) DLP as a function of local emission intensity at the center of the CNT film in parallel (red) and perpendicular (blue) configurations for both the suspended (solid markers) and on-substrate (unfilled markers) devices. The DLP is defined as DLP =  $(I_{\parallel}-I_{\perp})/(I_{\parallel}+I_{\perp})$ . The onsubstrate DLP maximum is ~0.6, and the suspended DLP maximum is ~0.9. At high emission intensity (high temperature), the DLP values of both suspended and on-substrate emitters reach the asymptotic value of ~0.25 (green dashed line).

dependences of the light emission in parallel and perpendicular suspended devices. In both devices, thermal emission appears polarized parallel to the CNT alignment direction, indicating that the polarized thermal emission arises from the high degree of CNT alignment. As shown in Figure 4a,b, the angular dependence was fitted by  $I_{\perp} - (I_{\parallel} + I_{\perp}) \cos^2(\vartheta - \varphi)$ , where  $I_{\parallel}$ and  $I_{\perp}$  are the polarized light intensities,  $\vartheta$  is the polarizer angle to which the intensity is measured, and  $\varphi$  is a correction parameter. The polarizer orientation is initialized with the current direction and rotated at an interval of 10°. The DLP was calculated through DLP =  $\frac{I_{\parallel} - I_{\perp}}{I_{\parallel} + I_{\perp}}$ . In Figure 4c, the DLP values are reported as a function of  $I_{\parallel}$  for both on-substrate and suspended devices. In concordance with Matano et al.<sup>24</sup> who reported linear polarization from CNT film, the maximum DLP value reached by on-substrate thermal emitters is 0.6. Conversely, by employing a suspended architecture, the aligned CNT film thermal emitters exhibit an enhancement of the polarization of the emitted light with a maximum DLP

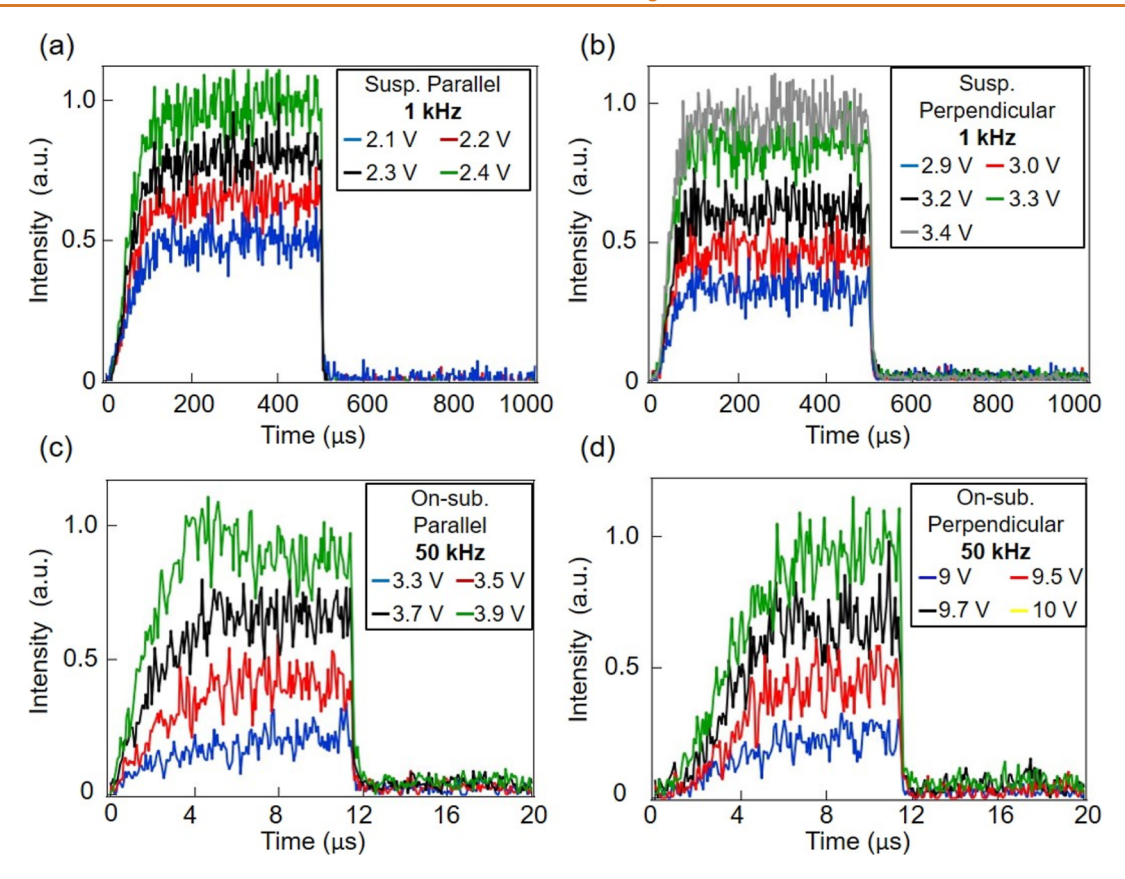


Figure 5. Time-resolved emission intensities in the suspended and on-substrate CNTs film devices under rectangular voltage: (a) emission intensities on the suspended parallel device measured at 1 kHz (2.1–2.4 V), (b) emission intensities on the suspended perpendicular device measured at 1 kHz (2.8–3.4 V), (c) emission intensities on the on-substrate parallel device measured at 50 kHz (3.3–3.9 V), and (d) emission intensities on the on-substrate perpendicular device measured at 50 kHz (9–10 V). These measured signals were fitted with a negative exponential function (see Section 4.2, Supporting Information) to estimate the relaxation times and characterize the thermal response behavior of the CNT film in the different configurations.

value of 0.9 for both parallel and perpendicular configurations. The reason for the enhanced polarization lies in the absence of the  $\mathrm{SiO}_2$  under the film. The on-substrate emitters are subjected to vertical heat dissipation through the oxide layer and, consequently,  $\mathrm{SiO}_2$  is heated and emits unpolarized thermal radiation, thereby causing the DLP to decrease. Furthermore, for the suspended devices, the DLP values decrease with increasing the light intensity and the film temperature as well as for the on-substrate devices reported in ref 24. The DLP asymptotically approaches  $\sim$ 0.25 in the high-temperature limit due to a 1D-to-3D crossover of carrier states. Therefore, a larger degree of polarization was achieved with suspended CNT film emitters, highlighting the prospective utility of the CNT film as a cutting-edge solution for applications reliant on light polarization.

We performed a time-resolved measurement to understand the thermal response speed of the films under square electric impulses for both on-substrate and suspended devices. A function generator was used to apply the electric impulses to the devices at 1 kHz for the suspended emitters and 50 kHz for the on-substrate emitters. As shown in Figure 5, the experimental results revealed that both the suspended (Figure 5a,b) and on-substrate (Figure 5c,d) devices exhibit fast exponential decay of the CNTs film temperature once the input voltage is off. The temperature decay was fitted by a negative exponential function proportional to  $\exp\left(-\frac{t}{\tau}\right)$ , where  $\tau$  is the relaxation time (see Section 4.2, Supporting

Information). The suspended devices present relaxation time values of about a few microseconds (5.7  $\mu$ s parallel, 9.7  $\mu$ s perpendicular), while the on-substrate devices have a relaxation time value of about hundreds of nanoseconds (0.11  $\mu$ s parallel,  $0.17 \mu s$  perpendicular). As explained in our previous work (ref 25), the parallel configurations show a faster response speed rather than the perpendicular ones in both suspended and onsubstrate structures because of the larger thermal conductivity along the channel direction that leads to faster thermal transport. However, the response speeds of the suspended structures are 1 order of magnitude larger than the respective on-substrate ones. This difference is explained by the presence of SiO<sub>2</sub> in the on-substrate structures. SiO<sub>2</sub> plays a crucial role because it advantageously allows heat to dissipate vertically from the CNT film; therefore, the relaxation time is shortened, leading to a faster response speed. Conversely, in the suspended structures, heat dissipation occurs only at the interface between SiO<sub>2</sub>/CNT/electrodes. As a result, the heat becomes more confined within the film, resulting in a longer relaxation time. In addition, the presence of SiO<sub>2</sub> affects the difference in response speed between parallel and perpendicular configurations. In the on-substrate devices, since the dominant heat transport is vertically through the substrate, the effect due to thermal conductivity anisotropy is limited, and the difference ratio in relaxation time between parallel and perpendicular configurations is about 1.5. Instead, in the suspended devices where the dominant heat transfer occurs

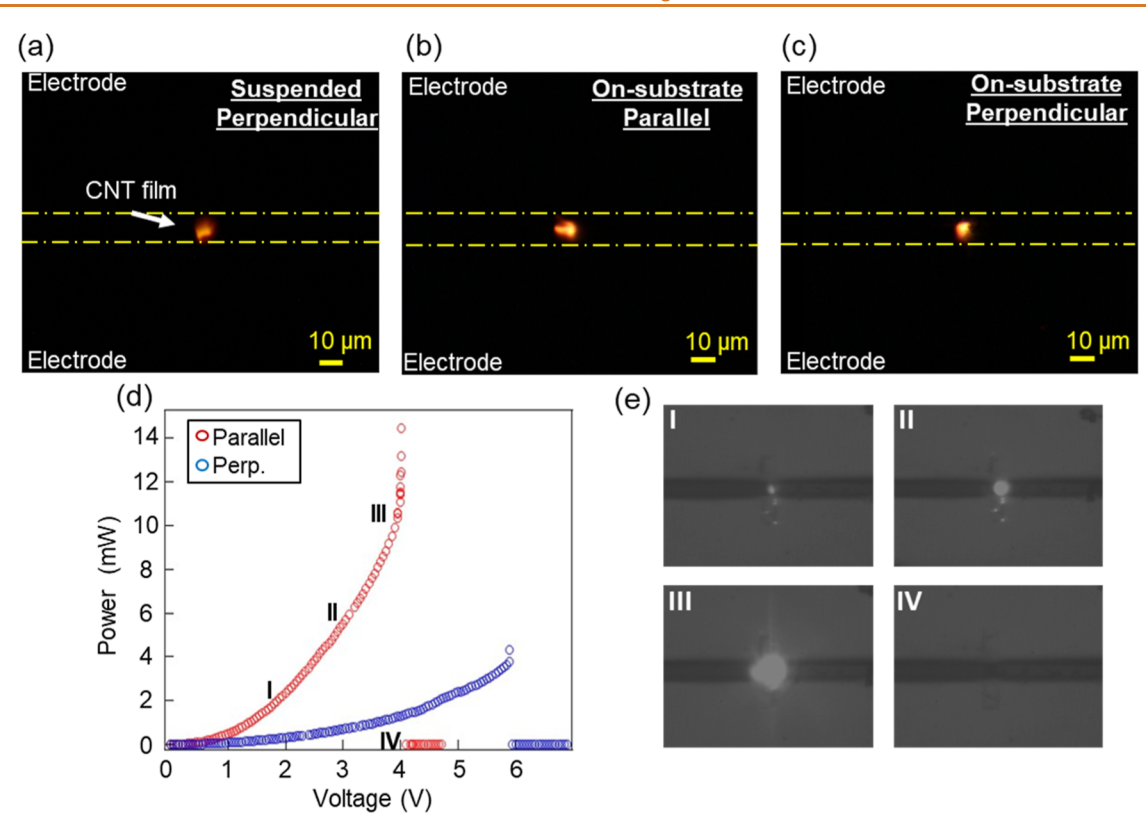


Figure 6. Visible light emission from CNT film emitters and breaking down at high operating temperatures: bright visible emission images of (a) suspended perpendicular device, (b) on-substrate parallel device, and (c) on-substrate perpendicular device These were observed with a visible camera. (d) Power—voltage characteristics of the parallel (red) and perpendicular (blue) suspended emitters until the breaking point. The numbers I—IV correspond to the IR camera pictures of the parallel suspended device during emission, reported in (e): (I) beginning of the emission. The light is irradiated from the center of the suspended film and from spots at the film/electrode interfaces. (II) The light intensity increases as the applied power is increased. (III) At high power, the bright spots at the film/electrode interfaces disappear, while the emission at the center of the film becomes brighter and unstable. The disappearance of the bright spots at the film/electrode interfaces corresponds to the improvement of the electric contact at SiO<sub>2</sub>/CNTs film/electrode interfaces. (IV) Breaking point and stop of light emission.

from the center of the CNT film to the electrode interfaces, the thermal anisotropy becomes more relevant and induces a larger difference ratio in the relaxation time between the parallel and the perpendicular configurations, that is about 1.7.

We investigated the visible light emission from the CNT film obtained by sufficiently increasing the temperature through high electric power. The bright visible light emissions, illustrated in Figure 6, confirm the great potential of CNT film as a thermal emitter, for its capability to provide high emission intensity within a broad spectral range, spanning from the IR to the visible, as well as a good tolerance for high temperatures under elevated bias voltage conditions. Visible emission was observed on the perpendicular configuration for the suspended device (Figure 6a) and on the on-substrate thermal emitters in both alignment configurations (Figure 6b,c). In the parallel suspended case, the lack of visible light emission was attributed to a change in the electric contact resistance at the interface between the CNT film and electrodes during the heating process. 41,42 The contact between the suspended film and the metallic electrodes is purely ohmic, 43 and the heat is equally dissipated through the contacts, resulting in a parabolic temperature profile along the film. 44 In Figure 6d, the I-V characteristics of parallel and perpendicular suspended emitters are reported until the final mechanical failure point. During the biasing of the suspended parallel emitter, the initial emission occurs at the contact film

and metal (Figure 6e-I). By increasing applied power, the suspended area of the CNT film is sufficiently heated to emit light (Figure 6e-II). With a further increase in the applied voltage, the light spots at the CNT/metal interface disappear, the current oscillates and increases, and instantaneous and intense emission occurs (Figure 6e-III), 42 as a result of the breakdown of the CNT film (Figure 6e-IV). The light emission before breaking is very strong but also very fast. 45 In the parallel configuration, since electrical and thermal conductivities are larger along the conduction channel, the electrical current is generally larger, as well as the heat dissipated through the electrodes, compared to the perpendicular configuration. This suggests that the film/electrode contacts are subjected to thermal stress, affecting their microstructures and generating an improvement in the contact. The electric characteristic of the parallel suspended emitter presents a pronounced power increase before the breakdown event that presumably arises from the contact improvement. The improvement of the contact leads to a decreased electrical resistance at the interface, with a consequently larger current flow within the film. This sudden large current flow film implies a rapid rise of the temperature that appears as a very bright light emission and the final breakdown. In other words, the temperature reaches immediately the maximum value sustainable by the tubes and causes the final breakdown. On the contrary, in the perpendicular configuration, the break-

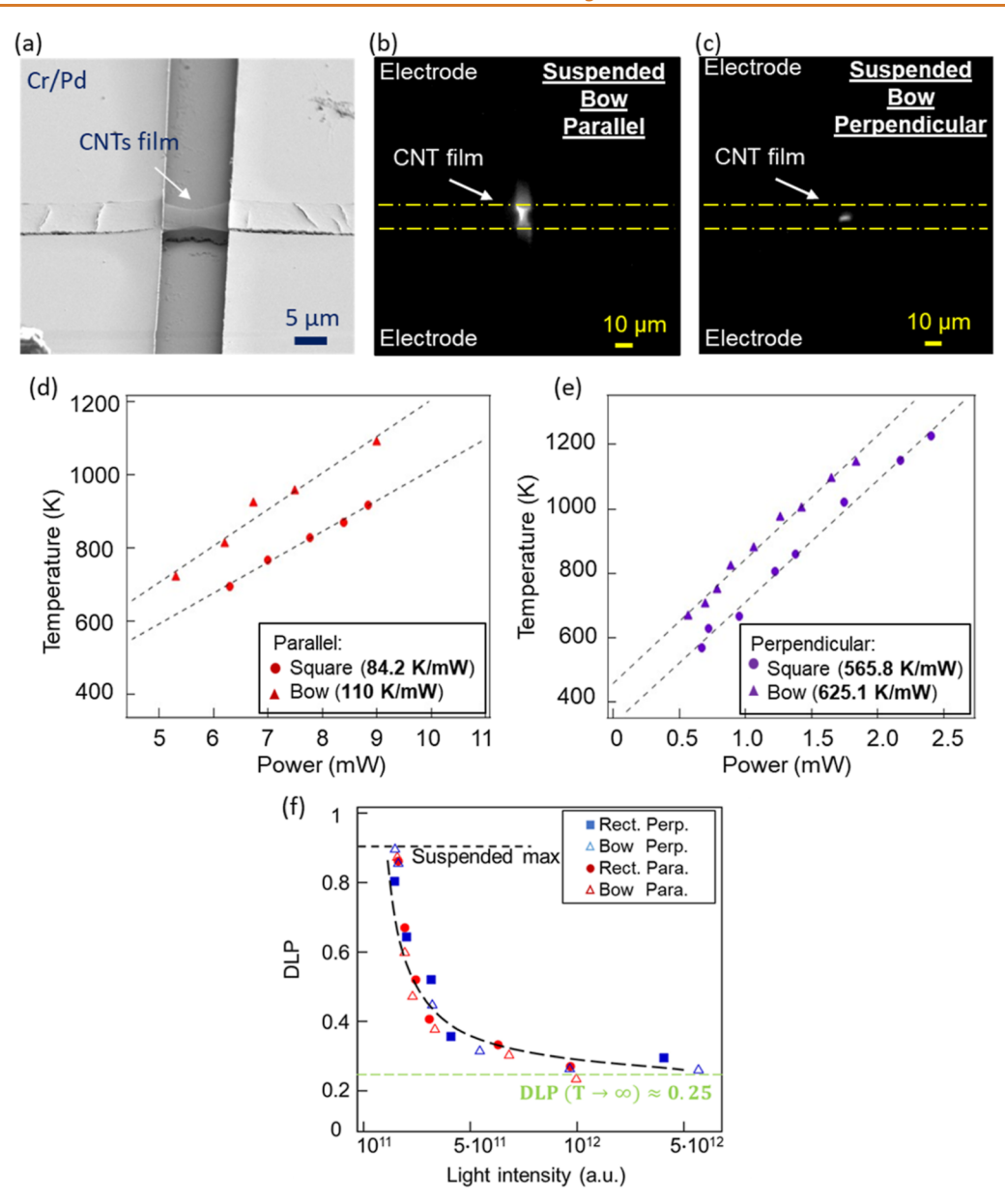


Figure 7. Thermal light emission and enhanced heating from "bow-shaped" suspended thermal light emission: (a) SEM images of the bow-shaped suspended CNT film with geometrical constrictions of 2.5  $\mu$ m. Infrared light emission of suspended bow-shaped emitters in parallel (b) and perpendicular (c) configurations. Device temperatures were calculated as a function of applied power for the bow-shaped device (triangles) and compared with those of the square device (circles) in parallel (d) and perpendicular (e) configurations. The dashed lines are linear fits that can be used to estimate the thermal performance factors. In both cases, the introduction of geometrical constrictions in the CNT film shape enhanced these factors. (f) DLP as a function of local emission intensity of parallel (red) rect. (circles) and bow (triangles) devices and perpendicular (blue) rect. (squares) and bow (triangles). The highest DLP value is  $\sim$ 0.9 in all configurations.

down point is reached gradually with the increase in the applied power. Even if the improvement of the interface contact occurs rapidly, the electric resistance of the conduction channel is still high and, therefore, no fast, abrupt bright emission was detected. The observation of the electric curve of the parallel suspended emitter suggests the presence of a power threshold that must be exceeded for the initiation of the breakdown. This value is approximately 10 mW and corresponds to a current density of the order of 10<sup>5</sup> A cm<sup>-2</sup>. As we consider pathways to achieve visible emission on the suspended parallel device, a promising solution is to shorten the CNT film's longitudinal length. The maximum current density just before breakdown is inversely proportional to the length of the film; therefore, the enhancement of the

breakdown current density will make the parallel suspended structure more resistant to string electric stressing and able to emit visible light.

We reported an enhancement of the thermal performance by adding geometrical constrictions (2.5  $\mu$ m) to the width of the CNT film. The devices, defined as "bow-shaped" (Figure 7a), exhibited an increase in the current density at the center of the film, where the constrictions are located, leading to higher operating temperatures and enhanced thermal performance factors. NIR emission of suspended bow-shaped devices for both parallel and perpendicular configurations, under a DC bias voltage are shown in Figure 7b,c, respectively. As for the square devices, we estimated the bow-shaped device temperatures through the blackbody spectra and compared the

temperature profiles against the applied electric power of bowshaped and square-shaped devices in both parallel (Figure 7d) and perpendicular (Figure 7e) configurations. At the same applied electric power, the bow-shaped devices reached higher temperatures than the square-shaped devices. Consequently, they exhibited brighter emission at locations corresponding to the geometrical constrictions and larger thermal performance factors, i.e., 110 and 625 K mW<sup>-1</sup> for the parallel and perpendicular configurations, respectively. Bow-shaped, suspended emitters exhibited a maximum DLP value of ~0.9 in both the parallel and perpendicular configurations, similar to the rectangular suspended devices (Figure 7f). The DLP value asymptotically approached ~0.25 in the high-temperature limit. The bow-shaped devices emit highly polarized light with DLP values comparable to those of rectangular devices but with enhanced heat performance.

# **CONCLUSIONS**

In this study, we successfully explored the measurement of highly polarized and efficient light emission from suspended thermal light emitters fabricated using aligned CNT films. The suspended structures exhibited improved thermal performance factors compared to the on-substrate devices. Furthermore, we found that the absence of a SiO2 underlying layer leads to interference between the light emitted from the CNT film and the light reflected by the Si substrate. The interference effect can be exploited to selectively enhance the thermal radiation at particular wavelengths where constructive interference was reported by appropriately engineering their trench depth. The greatest advantage reported from the suspended thermal emitters is a larger degree of linear polarization compared to the on-substrate structures, which indicates that this device brings out the film's potential for polarized light emission. Therefore, the suspended emitters offer the capability to directly generate highly polarized light by using microscale structures on a silicon chip. Unlike laser radiation, our devices emit polarized light across a wide spectral range, potentially useable for practical applications in fields, such as optoelectronics, photonics, and telecommunication. We analyzed the thermal response of the suspended and on-substrate devices under square electric signals, which shows the enhanced anisotropic effect due to the suspended structure, reflecting the characteristics of the CNT film. Additionally, visible light emission was obtained by applying high power, and the heatinduced breakdown was investigated for the device improvement. Interestingly, the visible light emission was not observed in the parallel configuration of suspended structures, allowing us to understand the behavior of CNT contacts once they are subjected to high thermal stress.

This work significantly contributes to the understanding of anisotropic light emission from thermal light emitters by using aligned CNT films. The advantages of the suspended structures, such as the high degree of polarization, improved thermal performance factors, and fast response speeds, make them promising candidates for various optical applications. The insights gained from this research enhance the development of advanced thermal light sources based on CNT alignment films, representing the possibility for future research and practical applications.

# **EXPERIMENTAL METHODS**

Fabrication. Highly aligned CNT films were prepared using a controlled vacuum filtration method. We obtained single-walled

carbon nanotubes with an average diameter of 1.4 nm from "Carbon Solution, Inc." (see Section 6, Supporting Information). To disperse the CNTs in water, we used sodium deoxycholate (Sigma-Aldrich) as a surfactant. To create devices based on these highly aligned CNT films, we started with a Si substrate covered by a 1.5  $\mu$ m SiO<sub>2</sub> layer. The aligned CNT films were transferred onto the substrate using a wet transfer process. In this process, the polycarbonate filter membrane was dissolved using chloroform to place the aligned CNT films onto the substrate. The aligned CNT film on the  $SiO_2/Si$ substrate was first patterned by photolithography and O2 plasma etching with a photoresist mask, which was subsequently removed by acetone. Cr/Pd electrodes with a gap of 10  $\mu$ m were formed as the source and drain electrodes on both ends of the film. The suspension of the film was obtained by removing the SiO2 layer through a semidry etching process based on HF acid. For more details, see Section 1 in the Supporting Information.

Optical Measurement System. Emission from the aligned CNT film devices was measured at room temperature and under vacuum conditions through a quartz optical window and a microscope objective lens. To perform optical measurements in the NIR region, the radiation was directed toward an InGaAs CCD camera and an InGaAs linear array detector equipped with a spectrometer. This setup allowed us to capture 2D emission images and emission spectra, respectively. The wavelength range detected was approximately from 900 to 1600 nm. To ensure accuracy, the relative spectral response of the measurement system, which included the optical path and the detector, was calibrated using standard light from a blackbody furnace and a thermal light bulb, and all collected spectra were adjusted accordingly. Polarization dependence of the emission intensity was measured by an InGaAs CCD camera and a polarizer. The timeresolved measurement was performed employing an objective lens and a multimode optical fiber that guides the light through an avalanche photodiode operating in Geiger mode for light detection and to an oscilloscope for light processing. See Section 3 in the Supporting Information for further details.

# **ASSOCIATED CONTENT**

# Supporting Information

The Supporting Information is available free of charge at https://pubs.acs.org/doi/10.1021/acsnano.4c02447.

Details on the device fabrication, optical measurement systems, basic calculation method for transient thermal 2D distribution in a CNT device, estimation method for the relaxation time of emission intensity, analysis of the effect of anisotropy of the CNT film on the emission, and discussion on the optical polarization (PDF)

# **AUTHOR INFORMATION**

# **Corresponding Author**

Hideyuki Maki — Department of Applied Physics and Physics-Informatics, Keio University, Yokohama 223-8522, Japan; Center for Spintronics Research Network, Keio University, Yokohama, Kanagawa 223-8522, Japan; orcid.org/0000-0001-5545-5932; Email: maki@appi.keio.ac.jp

#### **Authors**

Andrea Zacheo — Department of Applied Physics and Physico-Informatics, Keio University, Yokohama 223-8522, Japan; orcid.org/0009-0001-6553-6274

Shinichiro Matano — Department of Applied Physics and Physico-Informatics, Keio University, Yokohama 223-8522, Japan; orcid.org/0000-0001-5001-3203

Yui Shimura – Department of Applied Physics and Physico-Informatics, Keio University, Yokohama 223-8522, Japan
 Shengjie Yu – Department of Electrical and Computer Engineering, Rice University, Houston, Texas 77005, United

- States; Applied Physics Graduate Program, Smalley-Curl Institute, Rice University, Houston, Texas 77005, United States
- Jacques Doumani Department of Electrical and Computer Engineering, Rice University, Houston, Texas 77005, United States; Applied Physics Graduate Program, Smalley-Curl Institute, Rice University, Houston, Texas 77005, United States; Occid.org/0000-0002-2031-4918
- Natsumi Komatsu Department of Electrical and Computer Engineering, Rice University, Houston, Texas 77005, United States; Oorcid.org/0000-0003-0959-7088
- Junichiro Kono Department of Electrical and Computer Engineering, Rice University, Houston, Texas 77005, United States; Department of Physics and Astronomy and Department of Materials Science and NanoEngineering, Rice University, Houston, Texas 77005, United States;

  orcid.org/0000-0002-4195-0577

Complete contact information is available at: https://pubs.acs.org/10.1021/acsnano.4c02447

#### **Author Contributions**

 $\P$ A.Z. and S.M. contributed equally to this work.

#### Notes

The authors declare no competing financial interest.

#### **ACKNOWLEDGMENTS**

This work was partially financially supported by A-STEP (grant number JPMJTR20R4 and JPMJTR221B) and JST-Mirai Program (grant number JPMJMI22G6) from JST, and KAKENHI (grant number 20H02210) and Partnerships for International Research and Education (PIRE, grant number JPJSJRP20221202) from JSPS. This work was technically supported by the Spintronics Research Network of Japan, the Core-to-Core program from JSPS, and the NIMS Nanofabrication Platform in Nanotechnology Platform Project by MEXT. S.M. and Y.S. acknowledge support from JST SPRING (grant number JPMJSP2123), JSPS KAKENHI (grant number JP23KJ1913 and JP23KJ1903), and the Keio University Doctorate Student Grant-in-Aid Program from Ushioda Memorial Fund. N.K. and J.K. acknowledge support from the Robert A. Welch Foundation through grant number C-1509, the Air Force Office of Scientific Research through grant number FA9550-22-1-0382, the JST CREST program, Japan, through grant number JPMJCR17I5, the US National Science Foundation through grant number PIRE-2230727, and the Carbon Hub of Rice University.

#### REFERENCES

- (1) Gross, H.; Dörband, B.; Müller, H.; Gross, H., Dörband, B., Müller, H., Eds.; Wiley, 2015; .Handbook of Optical Systems, Metrology of Optical Components and Systems
- (2) Fujiwara, H. Spectroscopic Ellipsometry; Wiley, 2007; .
- (3) Berova, N.; Polavarapu, P. L.; Nakanishi, K.; Woody, R. W. Comprehensive 324 Chiroptical Spectroscopy: Applications in Stereochemical Analysis of Synthetic 325 Compounds, Natural Products, and Biomolecules; Wiley, 2012;
- (4) Kato, Y. K.; Myers, R. C.; Gossard, A. C.; Awschalom, D. D. Observation of the Spin Hall Effect in Semiconductors. *Science* **2004**, 306 (5703), 1910–1913.
- (5) Kato, Y.; Myers, R. C.; Gossard, A. C.; Awschalom, D. D. Coherent Spin Manipulation without Magnetic Fields in Strained Semiconductors. *Nature* **2004**, *427* (6969), 50–53.

- (6) Nakagawa, K.; Shimura, Y.; Fukazawa, Y.; Nishizaki, R.; Matano, S.; Oya, S.; Maki, H. Microemitter-Based IR Spectroscopy and Imaging with Multilayer Graphene Thermal Emission. *Nano Lett.* **2022**, 22 (8), 3236–3244.
- (7) Nakamura, S.; Sekiya, K.; Matano, S.; Shimura, Y.; Nakade, Y.; Nakagawa, K.; Monnai, Y.; Maki, H. High-Speed and On-Chip Optical Switch Based on a Graphene Microheater. *ACS Nano* **2022**, *16* (2), 2690–2698.
- (8) Nakagawa, K.; Takahashi, H.; Shimura, Y.; Maki, H. A Light Emitter Based on Practicable and Mass-Producible Polycrystalline Graphene Patterned Directly on Silicon Substrates from a Solid-State Carbon Source. *RSC Adv.* **2019**, *9* (65), 37906–37910.
- (9) Miyoshi, Y.; Fukazawa, Y.; Amasaka, Y.; Reckmann, R.; Yokoi, T.; Ishida, K.; Kawahara, K.; Ago, H.; Maki, H. High-Speed and on-Chip Graphene Blackbody Emitters for Optical Communications by Remote Heat Transfer. *Nat. Commun.* **2018**, *9* (1), 1279.
- (10) Kim, Y. D.; Gao, Y.; Shiue, R.-J.; Wang, L.; Aslan, B.; Bae, M.-H.; Kim, H.; Seo, D.; Choi, H.-J.; Kim, S. H.; Nemilentsau, A.; Low, T.; Tan, C.; Efetov, D. K.; Taniguchi, T.; Watanabe, K.; Shepard, K. L.; Heinz, T. F.; Englund, D.; Hone, J. Ultrafast Graphene Light Emitters. *Nano Lett.* **2018**, *18* (2), 934–940.
- (11) Kim, Y. D.; Kim, H.; Cho, Y.; Ryoo, J. H.; Park, C. H.; Kim, P.; Kim, Y. S.; Lee, S.; Li, Y.; Park, S. N.; Shim Yoo, Y.; Yoon, D.; Dorgan, V. E.; Pop, E.; Heinz, T. F.; Hone, J.; Chun, S. H.; Cheong, H.; Lee, S. W.; Bae, M. H.; Park, Y. D. Bright Visible Light Emission from Graphene. *Nat. Nanotechnol.* **2015**, *10* (8), 676–681.
- (12) Mori, T.; Yamauchi, Y.; Honda, S.; Maki, H. An Electrically Driven, Ultrahigh-Speed, on-Chip Light Emitter Based on Carbon Nanotubes. *Nano Lett.* **2014**, *14* (6), 3277–3283.
- (13) Takahashi, H.; Suzuki, Y.; Yoshida, N.; Nakagawa, K.; Maki, H. High-Speed Electroluminescence from Semiconducting Carbon Nanotube Films. *J. Appl. Phys.* **2020**, *127* (16), 164301.
- (14) Ma, Z.; Liang, S.; Liu, Y.; Wang, F.; Wang, S.; Peng, L.-M. On-Chip Polarized Light Emitters Based on (6,5) Chirality-Sorted Carbon Nanotube Aligned Arrays. *Appl. Phys. Lett.* **2016**, *108* (6), 063114.
- (15) Kinoshita, M.; Steiner, M.; Engel, M.; Small, J. P.; Green, A. A.; Hersam, M. C.; Krupke, R.; Mendez, E. E.; Avouris, P. The Polarized Carbon Nanotube Thin Film LED. *Opt. Express* **2010**, *18* (25), 25738.
- (16) Li, P.; Jiang, K.; Liu, M.; Li, Q.; Fan, S.; Sun, J. Polarized Incandescent Light Emission from Carbon Nanotubes. *Appl. Phys. Lett.* **2003**, 82 (11), 1763–1765.
- (17) Liu, P.; Liu, L.; Wei, Y.; Liu, K.; Chen, Z.; Jiang, K.; Li, Q.; Fan, S. Fast High-Temperature Response of Carbon Nanotube Film and Its Application as an Incandescent Display. *Adv. Mater.* **2009**, *21* (35), 3563–3566.
- (18) Wei, J.; Zhu, H.; Wu, D.; Wei, B. Carbon Nanotube Filaments in Household Light Bulbs. *Appl. Phys. Lett.* **2004**, 84 (24), 4869–4871
- (19) Estrada, D.; Pop, E. Imaging Dissipation and Hot Spots in Carbon Nanotube Network Transistors. *Appl. Phys. Lett.* **2011**, *98* (7), 073102.
- (20) Liu, Z.; Bushmaker, A.; Aykol, M.; Cronin, S. B. Thermal Emission Spectra from Individual Suspended Carbon Nanotubes. *ACS Nano* **2011**, *5* (6), 4634–4640.
- (21) Singer, S. B.; Mecklenburg, M.; White, E. R.; Regan, B. C. Polarized Light Emission from Individual Incandescent Carbon Nanotubes. *Phys. Rev. B* **2011**, *83* (23), 233404.
- (22) Mann, D.; Kato, Y. K.; Kinkhabwala, A.; Pop, E.; Cao, J.; Wang, X.; Zhang, L.; Wang, Q.; Guo, J.; Dai, H. Electrically Driven Thermal Light Emission from Individual Single-Walled Carbon Nanotubes. *Nat. Nanotechnol.* **2007**, 2 (1), 33–38.
- (23) Fan, Y.; Singer, S. B.; Bergstrom, R.; Regan, B. C. Probing Planck's Law with Incandescent Light Emission from a Single Carbon Nanotube. *Phys. Rev. Lett.* **2009**, *102* (18), 187402.
- (24) Matano, S.; Takahashi, H.; Komatsu, N.; Shimura, Y.; Nakagawa, K.; Kono, J.; Maki, H. Electrical Generation of Polarized

- Broadband Radiation from an On-Chip Aligned Carbon Nanotube Film. ACS Mater. Lett. 2022, 4 (4), 626-633.
- (25) Matano, S.; Komatsu, N.; Shimura, Y.; Kono, J.; Maki, H. High-Speed Modulation of Polarized Thermal Radiation from an On-Chip Aligned Carbon Nanotube Film. *Nano Lett.* **2023**, 23, 9817–9824.
- (26) He, X.; Gao, W.; Xie, L.; Li, B.; Zhang, Q.; Lei, S.; Robinson, J. M.; Hároz, E. H.; Doorn, S. K.; Wang, W.; Vajtai, R.; Ajayan, P. M.; Adams, W. W.; Hauge, R. H.; Kono, J. Wafer-Scale Monodomain Films of Spontaneously Aligned Single-Walled Carbon Nanotubes. *Nat. Nanotechnol.* **2016**, *11* (7), 633–638.
- (27) Komatsu, N.; Nakamura, M.; Ghosh, S.; Kim, D.; Chen, H.; Katagiri, A.; Yomogida, Y.; Gao, W.; Yanagi, K.; Kono, J. Groove-Assisted Global Spontaneous Alignment of Carbon Nanotubes in Vacuum Filtration. *Nano Lett.* **2020**, *20* (4), 2332–2338.
- (28) Fukuhara, K.; Ichinose, Y.; Nishidome, H.; Yomogida, Y.; Katsutani, F.; Komatsu, N.; Gao, W.; Kono, J.; Yanagi, K. Isotropic Seebeck Coefficient of Aligned Single-Wall Carbon Nanotube Films. *Appl. Phys. Lett.* **2018**, *113* (24), 243105.
- (29) Gao, W.; Doiron, C. F.; Li, X.; Kono, J.; Naik, G. V. Macroscopically Aligned Carbon Nanotubes as a Refractory Platform for Hyperbolic Thermal Emitters. *ACS Photonics* **2019**, *6* (7), 1602–1609
- (30) Green, M. E.; Bas, D. A.; Yao, H.-Y.; Gengler, J. J.; Headrick, R. J.; Back, T. C.; Urbas, A. M.; Pasquali, M.; Kono, J.; Her, T.-H. Bright and Ultrafast Photoelectron Emission from Aligned Single-Wall Carbon Nanotubes through Multiphoton Exciton Resonance. *Nano Lett.* **2019**, *19* (1), 158–164.
- (31) Yanagi, K.; Okada, R.; Ichinose, Y.; Yomogida, Y.; Katsutani, F.; Gao, W.; Kono, J. Intersubband Plasmons in the Quantum Limit in Gated and Aligned Carbon Nanotubes. *Nat. Commun.* **2018**, 9 (1), 1121.
- (32) Marconnet, A. M.; Panzer, M. A.; Goodson, K. E. Thermal Conduction Phenomena in Carbon Nanotubes and Related Nanostructured Materials. *Rev. Mod. Phys.* **2013**, 85 (3), 1295–1326.
- (33) Balandin, A. A. Thermal Properties of Graphene and Nanostructured Carbon Materials. *Nat. Mater.* **2011**, *10*, 569–581.
- (34) Kaiser, A. B. Electronic Transport Properties of Conducting Polymers and Carbon Nanotubes. *Rep. Prog. Phys.* **2001**, *64* (1), 1–49.
- (35) Wang, X.; Liu, Y.; Yu, G.; Xu, C.; Jinbiao, Z.; Zhu, D. Anisotropic Electrical Transport Properties of Aligned Carbon Nanotube Films. *J. Phys. Chem. B* **2001**, *105*, 9422–9425.
- (36) Pint, C. L.; Xu, Y.-Q.; Morosan, E.; Hauge, R. H. Alignment Dependence of One-Dimensional Electronic Hopping Transport Observed in Films of Highly Aligned, Ultralong Single-Walled Carbon Nanotubes. *Appl. Phys. Lett.* **2009**, 94 (18), 182107.
- (37) Jerome, B. B.; Prasad, C. S.; Schirato, A.; Dewey, O. S.; Doumani, J.; Baydin, A.; Gao, W.; Della Valle, G.; Kono, J.; Pasquali, M.; Naik, G. V.; Alabastri, A. Coupling into Hyperbolic Carbon-Nanotube Films with a Deep-Etched Antenna Grating. *ACS Photonics* **2023**, *10* (12), 4121–4132.
- (38) Luo, F.; Fan, Y.; Peng, G.; Xu, S.; Yang, Y.; Yuan, K.; Liu, J.; Ma, W.; Xu, W.; Zhu, Z. H.; Zhang, X. A.; Mishchenko, A.; Ye, Y.; Huang, H.; Han, Z.; Ren, W.; Novoselov, K. S.; Zhu, M.; Qin, S. Graphene Thermal Emitter with Enhanced Joule Heating and Localized Light Emission in Air. ACS Photonics 2019, 6 (8), 2117–2125.
- (39) Yamaguchi, S.; Tsunekawa, I.; Komatsu, N.; Gao, W.; Shiga, T.; Kodama, T.; Kono, J.; Shiomi, J. One-Directional Thermal Transport in Densely Aligned Single-Wall Carbon Nanotube Films. *Appl. Phys. Lett.* **2019**, *115* (22), 223104.
- (40) Yoon, D.; Moon, H.; Son, Y. W.; Choi, J. S.; Park, B. H.; Cha, Y. H.; Kim, Y. D.; Cheong, H. Interference Effect on Raman Spectrum of Graphene on SiO2/Si. *Phys. Rev. B: Condens. Matter Mater. Phys.* **2009**, 80 (12), 125422.
- (41) Saito, T.; Yamada, T.; Fabris, D.; Kitsuki, H.; Wilhite, P.; Suzuki, M.; Yang, C. Y. Improved Contact for Thermal and Electrical Transport in Carbon Nanofiber Interconnects. *Appl. Phys. Lett.* **2008**, 93 (10), 102108.

- (42) Costa, P. M. F. J.; Gautam, U. K.; Bando, Y.; Golberg, D. Direct Imaging of Joule Heating Dynamics and Temperature Profiling inside a Carbon Nanotube Interconnect. *Nat. Commun.* **2011**, 2 (1), 421.
- (43) Salazar, A.; Cardenas-Benitez, B.; Pramanick, B.; Madou, M. J.; Martinez-Chapa, S. O. Nanogap Fabrication by Joule Heating of Electromechanically Spun Suspended Carbon Nanofibers. *Carbon* **2017**, *115*, 811–818.
- (44) Santini, C. A.; Vereecken, P. M.; Volodin, A.; Groeseneken, G.; De Gendt, S.; Van Haesendonck, C. A Study of Joule Heating-Induced Breakdown of Carbon Nanotube Interconnects. *Nanotechnology* **2011**, 22 (39), 395202.
- (45) Collins, P. G.; Hersam, M.; Arnold, M.; Martel, R.; Avouris, P. Current Saturation and Electrical Breakdown in Multiwalled Carbon Nanotubes. *Phys. Rev. Lett.* **2001**, *86* (14), 3128–3131.